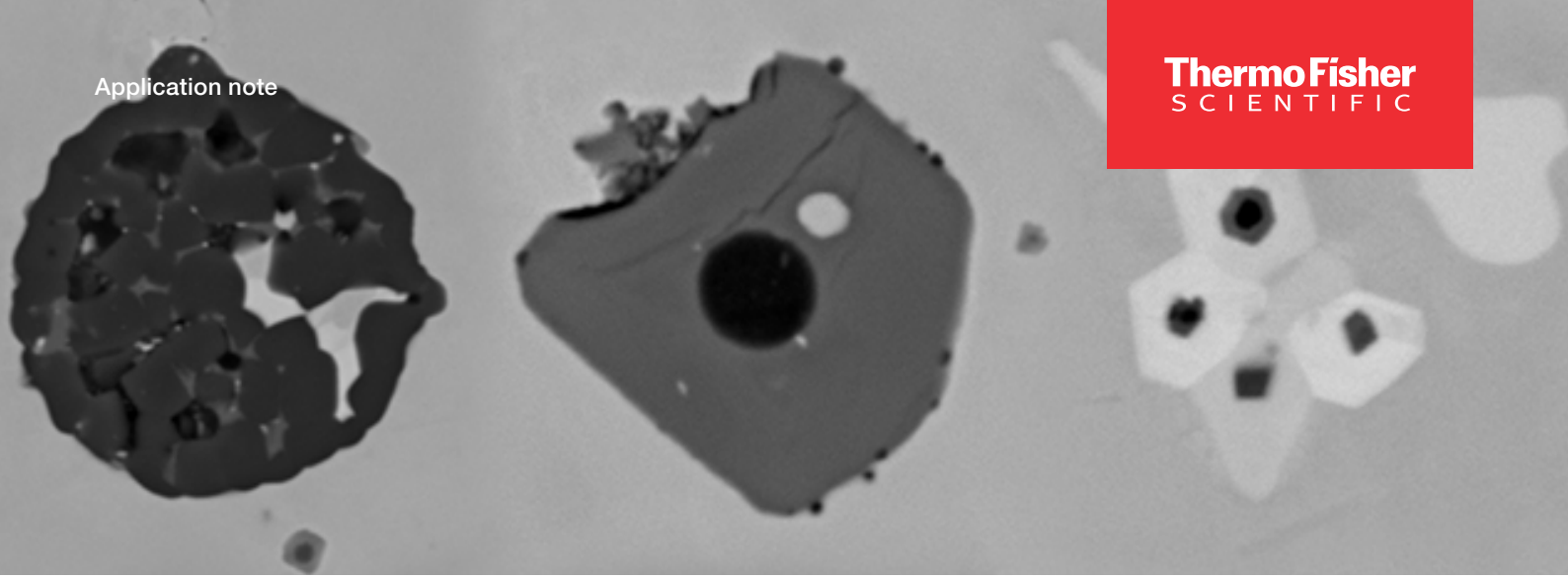

Application note

# Multiscale characterization of additive manufacturing alloys

## Identification of superalloy inclusions and precipitates with SEM and TEM

### Introduction

Metal additive manufacturing (AM) consists of rapidly melting and cooling alloys to build new structures layer by layer. This allows complex shapes to be produced with greater detail and less waste than traditional metal forging or machining. Potential AM methods include powder bed fusion, directed laser deposition (DLD), and wire arc AM. Powder-based methods will use spherical beads of a particular alloy that are approximately 20–120 µm in diameter; many of these belong to the aluminum, titanium, steel, and superalloy families.

In this application note, DLD was used to produce test specimens compositionally mimicking manufactured turbine blades in a turbofan engine. DLD directs a laser, powder particles, and inert gas through a nozzle to the same point in space on a substrate, which is particularly useful for the AM of parts, cladding one material onto another, or for repairing complex shapes.

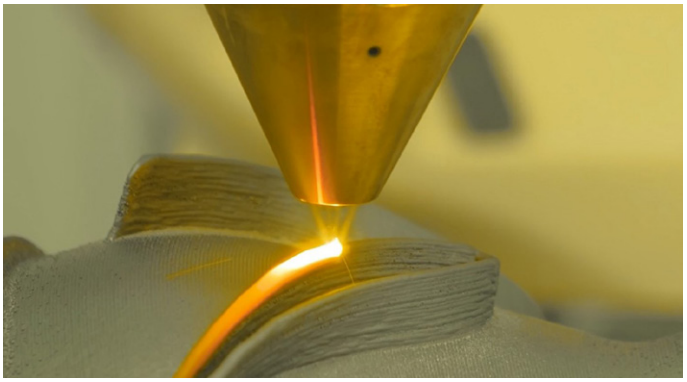

**Figure 1. Example of directed laser deposition (DLD) for metal additive manufacturing.**

The first stage of rotors in a turbine must withstand the highest thermal and mechanical loads of the engine, which is why nickel-based superalloys are often used for these parts, where resistance to creep and fatigue is especially important. In this study, DLD was used to produce test specimens of Alloy 718, a nickel-based superalloy that contains iron and chromium, to strengthen the austenitic base metal (γ). Additional alloying elements such as niobium, titanium, and aluminum are intended to combine with nickel to form nanoscale, semi-coherent precipitates ($Ni_3Nb$ γ" and $Ni_3(Ti,Al)$ γ') that provide much of the high-temperature creep and fatigue resistance. These samples were examined at both macro- and nano-scale with a combination of scanning (SEM) and transmission (TEM) electron microscopes.

| C | Ni | Cr | Fe | Nb | Mo | Ti | Si | Al |
|---|---|---|---|---|---|---|---|---|
| 0.4 | 51.0 | 19.2 | 17.9 | 5.6 | 3.1 | 1.2 | 0.6 | 0.4 |

**Table 1. Composition of Alloy 718 in weight percentages.**

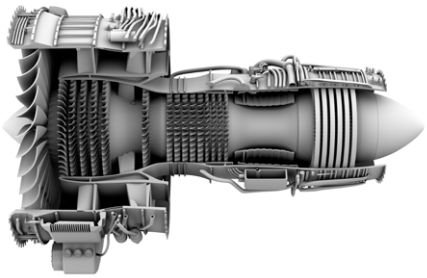

**Figure 2. A cross section of a passenger aircraft turbofan engine. Shown left to right: compression zones, the combustion zone, and the high temperature turbines.**

thermo scientific

## Methods

This application note seeks to evaluate the microstructure of test specimens in the as-built condition, which were produced at different laser speeds. For comparison, traditional processing routes may include casting, forging, and machining with multiple heat-treatment steps. The heat treatments are designed to dissolve unwanted phases while forming the desired γ" and γ' phases. With DLD as an alternative production route, we want to determine if the desired phases have formed, and if this method could be considered for part production, cladding, or repair.

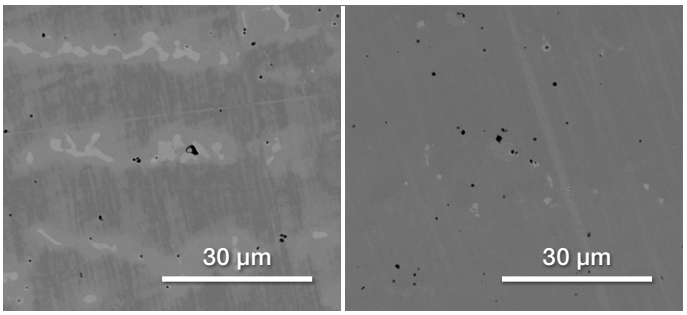


**Figure 3. BSE imaging from the slow (left) and fast (right) laser processing speeds.**

Three different laser processing speeds were used in this trial: 750, 1,000, and 1,250 mm/minute (further referred to as simply slow, medium, and fast). Vertical cross sections from each were mounted in resin and polished to a mirror finish. Manual and automated imaging were performed with the Thermo Scientific™ Phenom™ ParticleX™ Steel Desktop SEM. Backscattered electron (BSE) imaging reveals contrast relative to atomic weight, where heavier elements appear brighter and lighter elements are darker. Manual imaging of different laser speeds reveals a bright phase that is much more prevalent at the slow laser speed. Niobium has a much higher atomic weight than the nickel base metal (93 vs. 59), and it tends to segregate during melting. The brightest phase in Figure 3 was identified by energy dispersive spectroscopy (EDS) as niobium carbide (NbC), and areas surrounding the large NbC inclusions may have elevated niobium content in the base metal. In all, there were three different inclusion types recognized by their different BSE contrast.

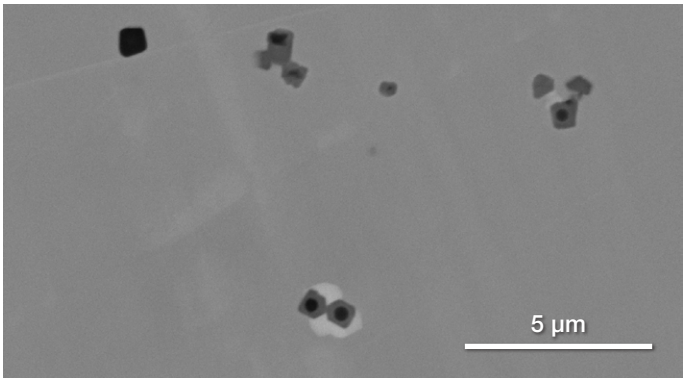


**Figure 4. BSE imaging at higher magnification shows various compound particles.**

## Quantifying microscale inclusions with SEM

Microscale inclusions can easily be quantified using automated workflows within the Phenom ParticleX Steel Desktop SEM; BSE image thresholds are selected to capture inclusions while excluding background material. Scans were merged at two different thresholds; one for bright particles and another for dark particles. Any inclusion greater than 2.0 µm in diameter in a 13 $mm^2$ area was characterized for shape, size, and composition. The ternary diagram in Figure 5 shows the composition distribution of TiN and $Al_2O_3$ inclusions in the fast-laser-speed sample. This can be interpreted as two compounds forming one upon the other, where the features in green are richer in TiN and the features in red are richer in alumina. These two types of inclusions did not appear to be affected by laser speed as their number, size, and composition were comparable across all three trials.

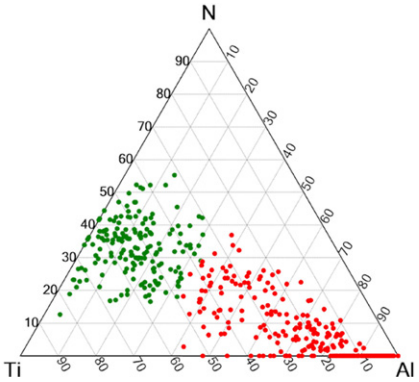


**Figure 5. Automated SEM imaging of the fast-laser-speed sample. The only classes shown in this Ti-Al-N ternary diagram are TiN in green and $Al_2O_3$ in red.**

The NbC inclusions, on the other hand, were far more prevalent in the slow-laser-speed trial; 497, 3, and 10 NbC inclusions per $mm^2$ were counted for the slow, medium, and fast trials respectively. Figure 6 shows ternary diagrams of the NbC inclusion distribution for the slow and fast laser speeds. This difference is attributed to the slow-laser-speed trial having increased time at elevated temperature, which allowed excessive segregation of niobium to occur. The medium and fast laser speeds were comparably low in their tendency to form NbC inclusions due to segregation.

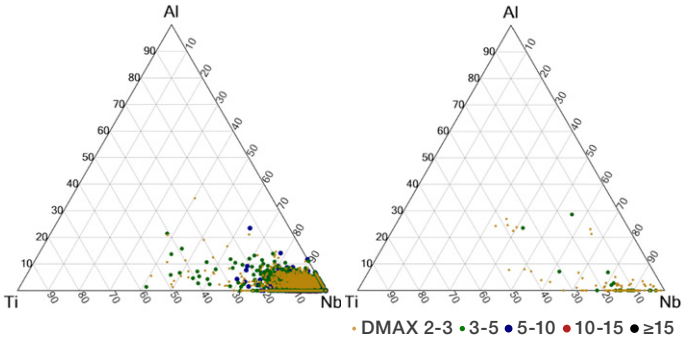


**Figure 6. Automated SEM imaging of the slow- and fast-laser-speed samples. Only the NbC class is shown on these Ti-Nb-Al ternary diagrams.**

Other artifacts were identified by image thresholding, but they lacked a sufficient EDS signal to be classified as an inclusion. Figure 7 shows several voids that were interpreted as gas bubbles or entrained metal splatter. DLD uses argon gas to transport metal powder to the melt pool, which may become entrained as bubbles. A splattered metal droplet could likewise be entrained into the pool, where it may not re-melt. Separate automated scans quantified the area fraction of voids to be 0.00036 (slow), 0.00014 (medium), and 0.00016 (fast).

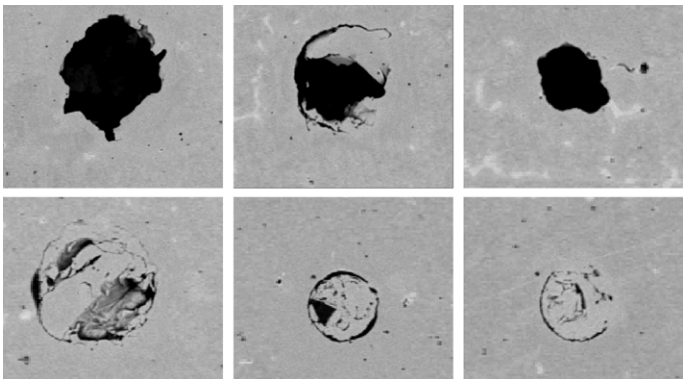

**Figure 7. Example BSE images automatically captured while searching for voids, with a size range around 10–40 µm. Holes may be gas bubbles, and dark halos suggest entrained metal splatter.**

## Quantifying nanoscale precipitates with TEM

Up to this point, several types of micron-sized particles and defects have been described. Nanoscale precipitates, which are responsible for the improvement in strength, still need to be identified. A further series of tests were conducted on the medium-laser-speed sample to uncover nanostructure with the Thermo Scientific™ Talos™ F200X TEM. As expected, there are inclusions comparable to those already observed, only smaller. Figure 8 shows a familiar core/shell structure of $Al_2O_3$ at the center, and TiN and NbC subsequently precipitating on top, as well as some very fine niobium concentrations in the bulk metal. At higher magnification, the oxide core is shown to contain fine spots of $ZrO_2$.

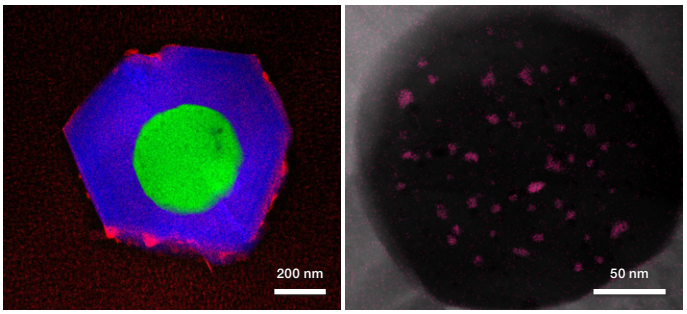


**Figure 8. TEM-EDS analysis on the left shows Nb (red), Ti (blue) and Al (green); a close up revealing Zr (pink) spots in the oxide core is shown on the right. *Courtesy of the University of Manchester.***

## Discussion

The Phenom ParticleX Steel Desktop SEM quantified the micron-sized NbC, TiN, and $A_{l2}O_3$ inclusions, as well as voids formed during manufacturing. At higher magnification in the Talos F200X TEM, very fine non-metallic precipitates were observed, and more definition was given to the lathe-like metallic precipitates. Figure 9 shows overlaid EDS maps of Al, Ti, and Nb; the corresponding light elements (O, N, and C) are also shown separately.

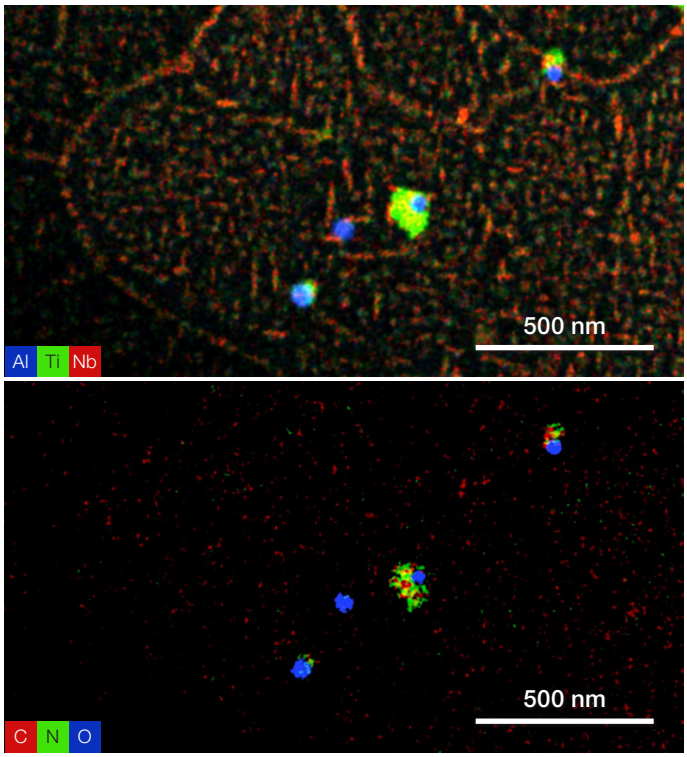


**Figure 9. TEM-EDS overlays of Al, Ti, and Nb (left) as well as C, N, and O (right).**

TiN precipitates were also quantified with the Thermo Scientific Automated Particle Workflow (APW). Figures 10 and 11 represent the particles characterized in a 25 $mm^2$ scan along with the associated size histogram. APW makes it possible to characterize nanoscale precipitate distributions in a short amount of time.

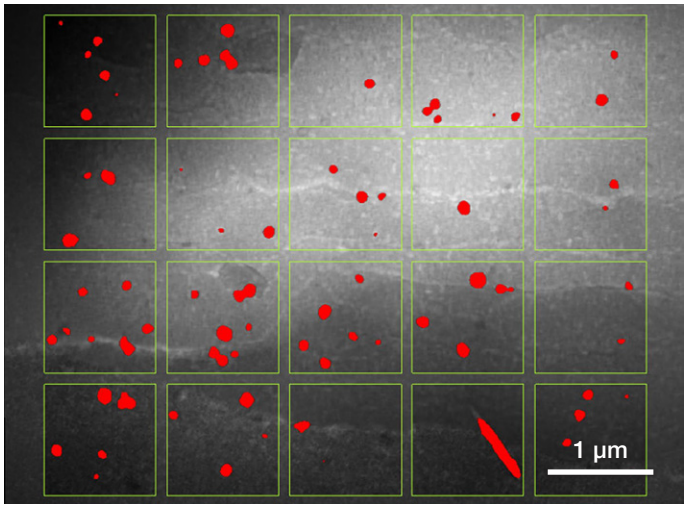


**Figure 10. Titanium particles characterized by APW.**

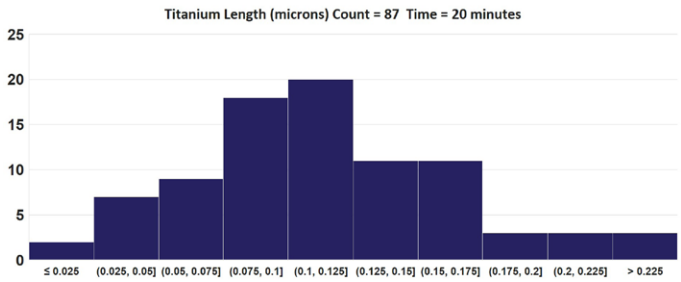


**Figure 11. Titanium particle histogram captured by APW.**

The semi-coherent precipitates of $Ni_3Nb$, or γ", are more challenging to quantify with EDS because the features are very thin and have much lower concentrations of Nb. Figure 12 shows the EDS map of Nb, and a characterization of the spectra by Automated eXpert Spectral Image Analysis, or AXSIA. The latter uses a multivariate statistical approach to determine principal components within the spectrum image. The bright regions on the AXSIA image are where a unique Ni + Nb spectrum (consistent with $Ni_3Nb$) is most concentrated. Note: the dark spots correspond to non-metallic precipitates where no $Ni_3Nb$ is present.

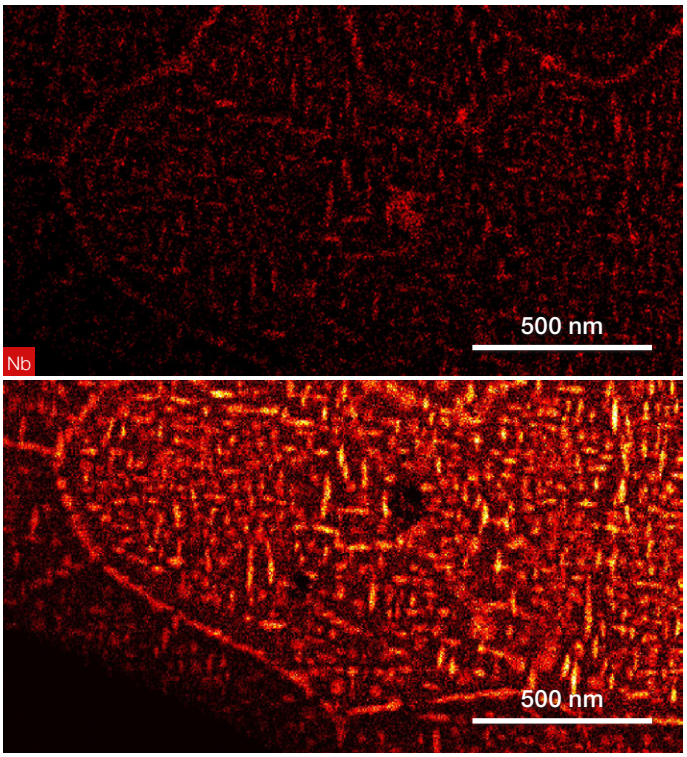


**Figure 12. Left: TEM-EDS map of Nb. Right: AXSIA component analysis for a Ni + Nb spectrum.** ***Courtesy of Sandia National Laboratories.***

Another way to confirm the presence of nanoprecipitates is with a selected area diffraction pattern. Figure 13 is a diffraction pattern which shows the base austenite structure and the γ" (combined with γ') superlattice reflections.

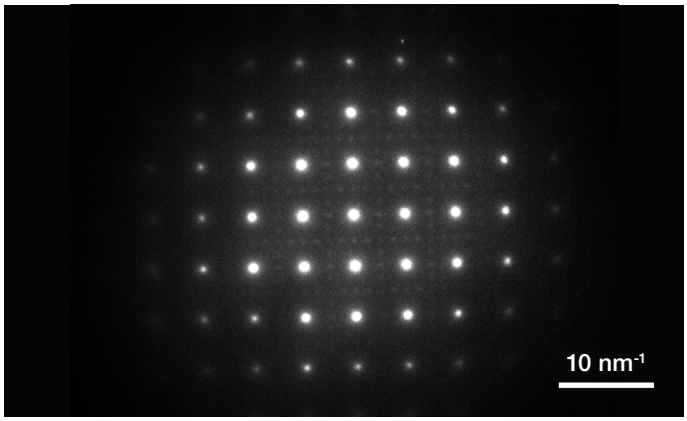


**Figure 13. TEM diffraction pattern showing γ matrix and γ" superlattice reflections.**

## Conclusions

Nickel superalloy test specimens were produced via directed laser deposition, an additive manufacturing technique. SEM, TEM, EDS, and diffraction techniques were combined to provide a full understanding of Alloy 718 at different laser speeds. The formation of the strengthening γ" phase in the as-built condition was positively shown with the Talos F200X TEM. Though this was successful, the unwanted brittle-phase NbC was also formed due to segregation and was most prevalent for the slow-laser-speed trial. The Phenom ParticleX Steel Desktop SEM quantified the micron-sized NbC, TiN, and $Al_2O_3$ inclusions, as well as voids formed during manufacturing. Electron microscopy instrumentation provided multi-scale, multi-modal characterization, identifying the benefits and limitations of DLD metal additive manufacturing.

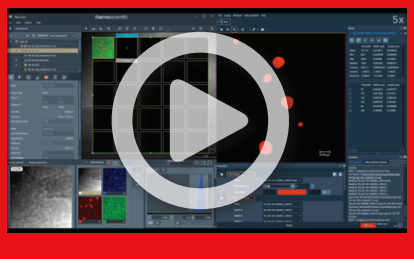

**Metals Research**

Duration 1:10

Learn more at **thermofisher.com/phenom-particle-x-steel**